

Paper to be presented at the Second International Congress for
Aeronautical Sciences to be held in Zurich, Switzerland
September 1960

EFFECTS OF NONEQUILIBRIUM FLOWS ON AERODYNAMIC HEATING
DURING ENTRY INTO THE EARTH'S ATMOSPHERE
FROM PARABOLIC ORBITS

By Glen Goodwin* and Paul M. Chung**
Glen Goodwin
National Aeronautics and Space Administration
Ames Research Center
Moffett Field, Calif.

INTRODUCTION

Entry into the earth's atmosphere at circular satellite speed has been studied extensively in recent years. As space voyages become more ambitious and atmosphere entry is made from the vicinity of the near planets or the moon, the entry speed will exceed circular satellite speed. It has been found by a number of investigators that as the entry speed increases, manned vehicles must fly through narrow corridors in order to enter the atmosphere in a single pass or to avoid excessive deceleration (see, e.g., refs. 1 through 4). Man's limited tolerance to deceleration and the requirement that entry be made during a single pass to avoid repeated voyages through the radiation belts restrict these entries to relatively shallow angles. These conditions result in the vehicle encountering intense convective heating at high speeds in the rarefied upper atmosphere.

It is the purpose of this paper to define in terms of vehicle parameters the realm of fluid mechanics where convective heating is most intense, to examine

*Chief, Heat Transfer Branch

**Aeronautical Research Scientist

the factors controlling the rate of convective heating for equilibrium flow, and to discuss the implication of nonequilibrium flow upon the convective heating rates experienced by these entry vehicles.

FLIGHT BOUNDARIES

To define the realm of fluid mechanics where the convective heating is most intense, it is helpful to define the allowable flight boundaries. As shown in the first figure, a space vehicle approaches the earth along a flight path which is a conic section until it encounters the earth's atmosphere, where the flight path will depart from the conic section because of aerodynamic forces. Two boundaries are apparent; the overshoot and the undershoot. The overshoot boundary is defined as the path where the vehicle just encounters enough atmospheric force to slow down sufficiently to enter in a single pass. Flight paths above this overshoot boundary result in multiple-pass entries with the vehicles making many excursions through the radiation belt. This situation is to be avoided for manned entry because of the weight penalty associated with shielding against this type of radiation. The lower or undershoot boundary is determined by deceleration limits, usually taken at 10 g for manned entry vehicles. If aerodynamic lift is employed during entry, these corridors can be deepened. Negative lift can be used to deflect the flight path downward and hence raise the overshoot boundary. In a similar way the use of positive lift can result in a lowering of the undershoot boundary since the vehicle can deflect its flight path upward and still make an entry without exceeding the deceleration limits specified.

It is convenient to define the corridor depths as the difference in conic perigee altitude between the overshoot and the undershoot boundary. Conic perigee is the perigee the vehicle would experience in the absence of an atmosphere. For

shallow entries the difference between the corridor depth defined this way and the actual depth in the outer edge of the atmosphere is small.

The depth of these entry corridors and hence the range of aerodynamic conditions these entry vehicles will encounter depend upon three parameters; maximum deceleration (G_{\max}), lift-drag ratio (L/D), and entrance speed (\bar{u}_1). For return trips from the vicinity of the moon, the resulting entry speed will be approximately escape speed or a speed ratio with respect to satellite speed of $\sqrt{2}$. The following discussion will be restricted to this entry speed.

It was mentioned earlier that vehicles capable of exerting aerodynamic lift could influence these corridor depths and hence increase the range of Reynolds number at which maximum convective heating occurs. The effect of aerodynamic lift on the depth of these corridors is shown in figure 2. In figure 2, corridor depth in miles is shown as a function of the lift-drag ratio of the vehicle. The corridors shown are for an entry for which L/D is held constant until the flight path becomes horizontal. At this time the maximum heating rate for the entry has been experienced by the vehicle. First, consider the lower region which is the corridor depth for nonlifting vehicles. This corridor is 7 miles wide for a vehicle experiencing maximum deceleration of 10 g. The middle shaded region represents the corridor deepening brought about by lowering of the undershoot boundary through the use of positive lift. For values of lift-drag ratio up to approximately unity, considerable deepening is evident. However, at higher values of lift-drag ratio the increase in corridor depth becomes relatively small. High values of lift-drag ratio become ineffective simply because the deceleration has been limited to 10 g. If a higher maximum deceleration can be tolerated, the rising trend of this curve persists to higher values of lift-drag ratio. The increase in corridor depth that results from raising the overshoot boundary by means of negative lift is shown by the upper

shaded region. Note that this use of negative lift is not as effective as the use of positive lift to lower the undershoot boundary. This results from the exponential nature of the atmospheric density variation with altitude. Above certain altitudes the vehicle is unable to produce sufficiently high force to deflect its flight path. It may be seen that the use of aerodynamic lift has increased these boundaries from 7 miles for the nonlifting vehicle to approximately 37 miles for a vehicle with a lift-drag ratio of one half.

It has been shown that entrance corridors can be deepened considerably by means of aerodynamic lift, and a reasonably deep corridor will certainly be necessary to allow for errors in vehicle guidance systems. The question is now raised as to what effect this corridor deepening has upon the aerodynamic heating and upon the nonequilibrium effects present in the flow field. Before discussing the aerodynamic heating in detail and the question of the effect of nonequilibrium flow upon the heating, it is of interest to review the regime of fluid mechanics wherein maximum convective heating occurs. The flight paths of representative vehicles entering the earth's atmosphere at escape speed are shown in figure 3. At the undershoot boundary, the flight path of a vehicle flying at lift drag ratios of $+1/2$ and 0 are shown; at the overshoot boundary, only the lift drag ratio $-1/2$ flight path is indicated. The examination of a large number of vehicle paths within the flight corridors previously discussed indicates that the region of maximum convective heating lies within an altitude band from 150,000 to 240,000 feet and over a relatively narrow speed range. The region of maximum heating is indicated in figure 3 by the crosshatched area, and it is the characteristics of the flow in this region that will now be examined. Two curves representing flight at a constant Reynolds number, Re , of 10^6 and 10^7 based on a 10-foot body length are shown in the figure. Flight paths above the upper curve result in Reynolds numbers less than a million, and flight paths below this line result in

Reynolds numbers greater than a million. Notice that the region of most severe convective heating occurs at Reynolds numbers generally less than one million and seldom exceeds about three million. It is probable, therefore, that the flow will be laminar. Also shown in figure 3 by the horizontal line labeled "Mean-free path $5/1000$ foot" is the region where rarefaction effects would be expected to become appreciable. It can be seen that in the region of most intense convective heating the flow is well within the continuum regime. It can be concluded from this figure, therefore, that in the region of most intense convective heating, the flow will most likely be laminar and continuum and for vehicles of reasonable size, ordinary boundary-layer equations should apply.

It is of interest to examine the flow in the region of intense convective heating to determine if the flow is in equilibrium. The states of the flow are shown in figure 4 in terms of altitude and velocity. The region of convective heating shown in the previous figure is indicated by the crosshatched rectangle. The solid line in the upper portion of the chart roughly divides the region of equilibrium and nonequilibrium inviscid flow. This line was determined for bodies with a one-foot nose radius by calculating for each velocity the point at which equilibrium was reached at the boundary-layer edge. Increases in nose radius would admittedly raise this line somewhat; however, the exact recombination rates are not known with great precision and it is felt that this line fairly well represents the division between equilibrium and nonequilibrium inviscid flow at the boundary-layer edge over the stagnation region of blunt bodies. Flight at velocities and altitudes below this line, then, result in flows which are in equilibrium at the boundary edge at the stagnation point. It appears, therefore, that the inviscid flow in the region of most intense convective heating will be substantially in equilibrium in the immediate region of the stagnation point.

The situation is somewhat different, however, when one examines the flow in the boundary layer. The state of flow in the boundary layer at the stagnation point is roughly indicated by the lower solid curve. Flights at altitudes below the second curve result in flows which are in chemical equilibrium. Notice, however, that a large portion of the region of intense convective heating is in the region where the flow in the boundary layer is somewhat out of equilibrium. Admittedly, the boundary between equilibrium and nonequilibrium is broad; this boundary was chosen at the point where convective heating on noncatalytic walls has been reduced some 30 percent below its equilibrium value by nonequilibrium effects.

Before presenting methods whereby the effect of nonequilibrium flow may be predicted, it is of interest to examine the characteristic of the heating history of a typical entry vehicle and to review the factors which influence the heating for the case of equilibrium flow. Nonequilibrium effects will then be treated as variations from the equilibrium case.

There is a fundamental difference between the heating rates encountered during an overshoot entry and those encountered during an undershoot entry. Figure 5 shows a typical heating history for a vehicle with a lift-drag ratio of $1/2$ and a W/C_DAR of 56 where R is the nose radius. In this figure are plotted stagnation-point heating rates as a function of time, for flight along the overshoot boundary and for flight along the undershoot boundary. Notice that the heating rate has a very high maximum at the undershoot boundary. The heating rate then drops to a low value and has a second maximum at a later time. The examination of a large number of calculated heating histories covering a wide range of entry conditions and vehicle parameters indicates that the first maximum is always the most severe and that, for all practical purposes, it occurs

when the ratio of the vehicle speed to satellite speed is equal to 1.3 for an entry made at a speed ratio equal to $\sqrt{2}$.

Along the overshoot boundary, the heating rates are reasonably low but persist for long periods of time. In most cases the total heat load experienced by the vehicle is greater along the overshoot boundary than along the undershoot boundary. The heating rate for this overshoot case does experience a gentle maximum at a speed ratio near 1.3, and this speed is unaffected by changes in vehicle parameters as was the case for the undershoot flight.

If it is assumed that the flow over these bodies is in chemical and thermodynamic equilibrium, it is possible to estimate the heating rates and heating loads by the following relatively simple relations which were obtained from reference 1.

The peak value of the stagnation point heating rate is given by

$$\dot{q} = \frac{19(C_q \bar{u}_1)^2 \sqrt{W/C_{DAR}} \sqrt{G_{max}}}{[1 + (L/D)^2]^{1/4}} \quad (1)$$

The constant C_q has been determined from electronic machine computations and varies from unity to about 0.60, depending upon the flight path. The actual values of C_q can be found tabulated in reference 1. The heat absorbed at the stagnation point as the vehicle decelerates from escape speed to satellite speed is given by

$$Q = \frac{8,800 \sqrt{W/C_{DAR}} [1 + (L/D)^2]^{1/4}}{C_Q \sqrt{G_{max}}} \quad (2)$$

The term C_Q has also been calculated and found to vary from unity to about 0.80, depending upon the flight path. The numerical values of C_Q are tabulated in reference 1. Note that both the heating rate and total heat absorbed depend directly upon the vehicle W/C_{DA} . The heavier vehicles for a given C_D and

base area experience both higher heating rates and higher total heating than do the lighter vehicles. Increase in lift-drag ratio can be seen to reduce the heating rate and to increase the heat absorbed. If the vehicle lift-drag ratio were independent of the drag coefficient, estimation of the heating rates for various vehicles under various flight conditions would be very simple. However, these two quantities are interrelated and, in general, vehicles with high lift-drag ratios will have small drag coefficients and, hence, high values of W/C_{DA} . However, for many practical cases these two factors may be treated separately for values of L/D up to approximately $1/2$.

The free-stream air density at the condition of maximum heating is a necessary quantity in determining the state of the flow over these re-entry vehicles. The density in ratio to sea-level density calculated by the method given by reference 1 is

$$\frac{\rho}{\rho_{sl}} = 1.26 \times 10^{-6} \frac{G_{\dot{q}_m} (W/C_{DA})}{\bar{u}_{\dot{q}_m}^2 [1 + (L/D)^2]^{1/2}} \quad (3)$$

At the condition of maximum convective heating the values of $G_{\dot{q}_m}$, $\bar{u}_{\dot{q}_m}$ are given below and were obtained from examination of computed flight paths along both the undershoot and overshoot boundaries.

<u>L/D</u>	<u>$\bar{u}_{\dot{q}_m}$</u>	<u>$G_{\dot{q}_m}$</u>
Undershoot boundary		
0	1.23	10
1/2	1.27	10
1.0	1.30	10
Overshoot boundary		
0	1.30	3.0
-1/2	1.30	1.3
-1.0	1.34	1.0

It can be seen from equation (3) that the density depends mainly upon the deceleration, the velocity ratio at maximum heating, the vehicle $W/C_D A$, and L/D . It is interesting to note that $W/C_D A$ is the parameter which most strongly affects the density at the condition of maximum heating rate at either the overshoot or undershoot boundary.

STAGNATION-POINT NONEQUILIBRIUM HEAT TRANSFER

The main conclusion from the preceding section was that vehicles entering the earth's atmosphere at escape speed along flight paths designed to permit safe manned occupancy experienced their maximum heating at a speed ratio of approximately 1.3 times satellite speed. This speed is reached at high altitudes where nonequilibrium effects would be expected. Nonequilibrium gas flows will now be investigated in some detail.

The subject of laminar heat transfer to blunt bodies in dissociated air has been treated extensively in the literature. Some of the more pertinent investigations are listed in references 5 through 8. The main results of these investigations indicate that there is little difference between heat-transfer rate when the flow is in equilibrium, partly out of equilibrium, or frozen if the catalytic efficiency of the vehicle wall is high. For high catalytic efficiency, all of the atoms that reach the wall recombine upon it and yield their heat of recombination to the wall. This result appears to hold whether the vehicle is constructed with a radiation heat shield or an ablation heat shield. This point is discussed in reference 9.

When the vehicle wall is noncatalytic and does not promote recombination reactions, a relatively large decrease in the heating rate can be achieved if the boundary layer is frozen or out of equilibrium. An indication of the magnitude of the change in the heating between the catalytic and noncatalytic wall

can be seen in figure 6 taken from reference 5. In this figure the Nusselt number divided by the square root of the Reynolds number is plotted against the recombination rate parameter for two assumed values of the wall catalytic efficiency. The upper curve, which shows essentially no variation of heating rate with recombination rate parameter, is for the highly catalytic wall. The lower curve is for the case where the wall is noncatalytic. The recombination rate parameter C defined in the figure is basically a function of the flight velocity, the flight density, and the vehicle nose radius and is physically the ratio of the time for an atom to diffuse through the boundary layer to the lifetime of the atom, sometimes termed "the chemical time." It is this parameter by which one can judge the amount of nonequilibrium effects present. For low values of the recombination rate parameter, the lifetime of the atom is long compared to the diffusion time and large numbers of atoms reach the surface where, if the wall is noncatalytic, no recombination takes place. Hence, a large fraction of the energy normally available for heat transfer to the body is not transferred to the surface.

An integral method was used in reference 10 to calculate the nonequilibrium effects on the heat transfer to blunt cones with noncatalytic walls. Numerical calculations were obtained over a wide range of flight speeds and altitudes. The results of reference 10 were used to obtain a general correlation that permits the prediction of heating rate at a stagnation point in the presence of nonequilibrium effects.

The analysis reported in reference 10 and used in the present paper to obtain this correlation is, however, subject to some basic limitations which will be discussed before the correlation is presented. First of all, the analysis of reference 10 was based on the specific recombination rate coefficient of

$3 \times 10^{16} (300/T)^{1.5}$, for both the oxygen and the nitrogen reactions. This expression was given in reference 11 for oxygen recombinations and agrees with the general level of the available experimental data. It appears that the specific recombination-rate coefficient of nitrogen may not be too different from that of oxygen because of their molecular similarity. However, the final authoritative experimental values are yet to be obtained. The variation of the recombination rate coefficient will affect the parameter C directly and, in turn, the heat transfer. Secondly, the analysis was performed for a wall temperature of 1500°K . If the wall temperature is decreased, the heat transfer increases as a result of the increased chemical activity near the cold wall. It was shown, for instance, in reference 10, that at a flight altitude of 200,000 feet and a velocity of 27,000 feet per second the stagnation point heat transfer increased from about 45 to about 60 percent of the equilibrium value when the wall temperature of a 5-foot nose radius decreased from 1500° to 1000°K . The nonequilibrium effect is, therefore, quite sensitive to wall temperature.

The present heat-transfer analysis did not consider the effect of ionization. Ionization is negligible up to the flight velocity of about 30,000 feet per second. At flight velocities above this value the effect of ionization may not be negligible. No information is available on the ionized nonequilibrium boundary layer at the present time, and therefore no attempt to predict the effect of the ionization will be made. A sufficient amount of ionization, however, could change the picture considerably, and work should be done on this problem.

Finally, the present study was concerned with convective heat transfer only. The radiative heat transfer may become important in certain flight regimes. At the particular flight conditions of interest in the present analysis, however, the convective heat transfer is the predominate part of the total heat transfer.

A summary correlation plot showing the effects of nonequilibrium on stagnation-point heating rate is shown in figure 7. In this figure the difference between the actual and frozen heating rate in ratio to the maximum possible difference in heating rate is shown as a function of a somewhat more complicated recombination rate parameter than was used in figure 6. The parameter, Γ , is the product of the ratio of the diffusion time to the atom lifetime and a correlation factor. The function of the correlation parameter, which depends upon the atom concentration behind the normal shock wave and the external flow at the boundary-layer edge, is to account for the effects of flight altitude and flight velocity. This correlation has been obtained from electronic machine computations over a range of velocities from 11,000 to 31,000 feet per second, altitude from 120,000 to 220,000 feet, atom concentrations at the boundary-layer edge from 0.075 to 1.0, for body-nose radii from 1 to 5 feet, and for one-wall temperature, 1500° K; this curve, then, can be used to determine quickly the effect of nonequilibrium flow on the heating rate to a stagnation point for various flight conditions.

Since figure 7 gives only the difference in heating rate between the equilibrium and the frozen flow, a relation giving the ratio between these quantities for various flight conditions is useful. While this relation may be obtained easily from references 5 and 6, it is given below for convenience.

$$\frac{\dot{q}_f}{\dot{q}_E} = \frac{h_{f_e} - h_{f_w}}{h_{t_e} - h_{t_w}} \quad (4)$$

For the conditions of interest to the present investigation the ratio is approximation 1/4.

The recombination rate parameter is, for the conditions of interest to this investigation, mainly a function of the free-stream density. The relation between Γ/R and the ratio of the air density to sea-level density is shown in figure 8

for flight speeds ranging from satellite speed to 1.27 times satellite speed.

A reasonably good representation of these calculated values of Γ/R is given by

$$\frac{\rho_{\infty}}{\rho_{sl}} = 3.65 \times 10^{-3} \left(\frac{\Gamma}{R} \right)^{0.563} \quad (5)$$

With the use of equations (3) and (5) the recombination rate parameter may be related to the vehicle characteristics as

$$\frac{\Gamma}{R} = 7.13 \times 10^{-7} \left[\frac{G \dot{q}_m (W/C_D A)}{\bar{u}_{q_m}^2 \sqrt{1 + (L/D)^2}} \right]^{1.77} \quad (6)$$

With the relation shown by equation (6) and the heat-transfer difference relations shown in figure 7, the effect of nonequilibrium flow on the maximum convective heating rate to the stagnation point of various vehicles may easily be determined.

The reduction in stagnation point maximum heating rate for nonlifting vehicles with noncatalytic walls as a function of $W/C_D A$ is shown in figure 9. A vehicle of 5-foot nose radius was chosen for the calculations shown in this figure. The upper curve represents flight at the undershoot boundary, and it can be seen that at the value of $W/C_D A$ greater than about 200 the flow is essentially equilibrium. For vehicles with a $W/C_D A$ less than 100, considerable reduction in heating ratio can be achieved if no recombination takes place on the vehicle wall. Along the overshoot boundary the flow tends to be nonequilibrium because of the higher flight altitudes. Again, as in the case of the undershoot boundary, the lighter vehicles exhibit more nonequilibrium effects than the heavier vehicles.

Vehicles with small nose radii will generally encounter nonequilibrium effects at lower altitudes than will vehicles with large nose radii for the same vehicle $W/C_D A$. This effect is shown in figure 10 for a nonlifting vehicle with a constant $W/C_D A$ of 100 but with a varying nose radius. At the undershoot boundary, the nose radius must be reduced to about 2 feet in order to achieve about 50 percent of the maximum possible benefit which could be gained if the flow were completely

frozen. Conditions along the overshoot boundary are somewhat more favorable. Reducing the nose radius to about 2 feet allows about 90 percent of the maximum benefit to be achieved if the vehicle wall is noncatalytic.

The use of lift results in a flight path which is deflected from the flight path followed by a ballistic vehicle and, as a consequence, can change the density and hence the amount of nonequilibrium flow at a stagnation point. The effect of L/D on heating conditions at the stagnation point is shown in figure 11 for a vehicle with a $W/C_D A$ of 100. Along the undershoot boundary, some reduction in the heating rate can be achieved if positive lift is employed. At the overshoot boundary, however, the situation is quite different. The boundary layer is substantially frozen even at an L/D of zero and little change is evident if negative lift is used to raise the flight boundaries.

The maximum stagnation heating rate along the undershoot boundary for the vehicle represented in figure 5 for L/D of $1/2$ is approximately 600 Btu/sec ft². If the vehicle wall were noncatalytic the heating rate would be reduced to about 330 Btu/sec ft², or roughly half of the equilibrium value by these nonequilibrium effects, which indicates that research on the problem of achieving noncatalytic walls might be fruitful.

NONEQUILIBRIUM EFFECTS ON AFTERBODIES

The preceding discussion was limited to the effect of departures from equilibrium on the stagnation point heating rate for a noncatalytic surface. The state of the boundary layer as it expands around the blunt nose and flows along the body will now be considered and the resulting changes in the heating rate will be discussed.

In reference 10 a modified form of the Von Kármán integral method was used to calculate the nonequilibrium heat transfer around cones with spherical tips.

Figure 12, taken from reference 10, shows a typical variation of nonequilibrium heat transfer around the body expressed as a fraction of the equilibrium value. This particular figure is for the flight altitude of 150,000 feet and the velocity of 26,000 feet per second. In the calculation, the inviscid flow along the edge of the boundary layer was assumed to be chemically frozen at its stagnation-point value, and this assumption is believed to be realistic. It is seen, for instance, when the nose angle is 70° that the chemical reaction rate freezes rapidly around the nose, as indicated by the reduction in heating rate, and recovers very slowly along the conical afterbody. The local heat transfer around the body can deviate substantially from that at the stagnation point. The effect of changing the nose radius from 3 feet to 1 foot can be seen by comparing the solid-line curve with the dashed-line curve which was calculated for the smaller nose radius body. The flow is farther out of equilibrium at the stagnation point, as discussed earlier, for the smaller nose radius body than for the larger radius and the effect persists back at least to four nose radii.

It appears from the results shown in this figure and from the results reported in reference 10 that the condition of the flow at the stagnation point is a reasonably good indication of the state of the flow over the rest of the body.

The analysis of reference 10 leading to a result such as that in figure 12 involves a substantial amount of numerical work. The possibility of using a simple method to predict qualitatively the chemical behavior of boundary layer around a body will now be considered. Figures 6 and 7 show that the most important parameter controlling the chemical state of a boundary layer at the stagnation point is the ratio of the diffusion time to the chemical time, $\frac{\tau_{diff}}{\tau_{chem}}$. It appears, therefore, that the variation of this ratio along the body will, to a first approximation, show the variation of the chemical state of the boundary layer.

The diffusion time can be obtained with the aid of reference 10 as

$$\left(\frac{\tau}{\tau_0}\right)_{\text{diff}} \approx \begin{cases} \frac{1}{f(X)} & \text{for } X \leq \theta \\ \frac{X}{\theta f(X)} & \text{for } X > \theta \end{cases} \quad (7)$$

where

$$f(X) = \frac{\rho_e \mu_e u_e r^{2\epsilon} X}{4 \int_0^X \rho_e \mu_e u_e r^{2\epsilon} dX} \quad (8)$$

If Newtonian theory is used to relate the pressure to the body shape, $f(X)$, and therefore the ratio $\left(\frac{\tau}{\tau_0}\right)_{\text{diff}}$, becomes a function only of the distance X and does not involve flight conditions.

The chemical reaction time will be considered next. The recombination process, according to the third-order chemical kinetics, is roughly proportional to the square of the density. The recombination rate is maximum, therefore, near the cooled wall where the density is maximum. The variation of the reaction rate around the body may be approximated by the variation of ρ^2 along the wall. The density along the wall varies roughly with the pressure for walls at near uniform temperature. The variation of the chemical reaction time is, therefore, approximately represented by the variation of pressure squared as

$$\left(\frac{\tau}{\tau_0}\right)_{\text{chem}} \approx \left(\frac{p_0}{p}\right)^2 \quad (9)$$

The variation of the ratio of the diffusion to the chemical times from equations (7) and (9) is shown in figure 13 for the two nose angles of 50° and 70° . A comparison of $\frac{\tau_{\text{diff}}}{\tau_{\text{chem}}}$ from figure 13 with \dot{q}/\dot{q}_E from figure 12 shows that the qualitative chemical behavior of the boundary layer is quite well predicted around the body by the simple analysis.

It is interesting to determine if the relationship between the recombination rate parameter and the heating rate at the stagnation point shown on figure 7 can be extended to include the afterbody flow. Figure 7 shows the relationship between the heat-transfer ratio $\frac{\dot{q} - \dot{q}_f}{\dot{q}_E - \dot{q}_f}$ and the parameter Γ at the stagnation point for a rather wide range of flight conditions. If it is assumed that the same relationship holds for all X , then figures 7 and 13 will enable one to calculate nonequilibrium heat transfer around the body. The result of this comparison is shown in figure 14. The results of the more complete calculation method shown in figure 12 are transferred to the present figure as the solid-line curve and the dashed-line curve. The results of the simplified method are shown by the open symbols. It is seen that this approximation predicts heat transfer quite accurately as the boundary layer expands around the nose, where the flow was still expanding to a lower pressure. Along the conical afterbody, however, the simple method predicts that the flow recovers to its equilibrium value faster than is indicated by the more complete calculation. The method does, however, yield conservative results.

CONCLUDING REMARKS

The flight paths of vehicles entering the earth's atmosphere from parabolic orbits have been examined in a general way and it is evident that the most intense aerodynamic heating will be encountered over a very narrow speed range and at high altitudes. The heating is thus most intense at conditions under which boundary-layer flows would be expected to exhibit nonequilibrium effects.

Since most methods of calculating nonequilibrium effects involve considerable numerical calculation, a simple method is developed which permits easy estimation of the effect of nonequilibrium on the heating rate to a stagnation point in terms of vehicle aerodynamic parameters. Specifically, it has been found that

(a) For flights along a 10 g deceleration-limited undershoot boundary, the stagnation-region boundary-layer flow is nonequilibrium for vehicles with $W/C_D A$ less than 100 and with nose radii less than 5 feet.

(b) Along an overshoot boundary which just permits entry during a single pass, the flow is nearly frozen at the stagnation point for vehicles with $W/C_D A$ less than 100 for both the lifting and nonlifting cases.

It is then shown that as the flow expands around the blunt nose, and along the afterbody considerable freezing of the flow takes place.

A method is developed whereby the effect of the nonequilibrium boundary-layer flow on the heating rate to the afterbody downstream of the nose can be estimated. This method is quite accurate in the expanding region downstream of the nose but predicts that the flow recovers its equilibrium more quickly on the conical afterbody than indicated by the more complete calculation method.

LIST OF SYMBOLS

A	vehicle reference area used to determine C_D
C	recombination rate parameter defined in figure 6
C_D	vehicle drag coefficient
C_Q	coefficient in total heat equation taken from reference 1
C_q	coefficient in heating rate equation taken from reference 1
c	total mass fraction of atoms
c_1	mass fraction of oxygen atoms
c_2	mass fraction of nitrogen atoms
c_p	frozen specific heat of the gas mixture
G_{max}	maximum resulting deceleration, g units
G_{dm}	deceleration at maximum heating, g units

g	earth's gravity acceleration, 32.2 ft/sec ²
h_f	frozen total enthalpy defined by $\frac{u_\infty^2}{2} + \int_0^T c_p dT$
h_t	total enthalpy defined by $h_f + \Delta h^0$
Δh^0	average heat of recombination
K_0	constant used in figure 7
Le	Lewis number
L/D	vehicle-lift-drag ratio
P	pressure, atm
Nu	Nusselt number
Q	stagnation point heat absorbed
\dot{q}	heating rate
R	nose radius, ft
Re	Reynolds number
R_u	universal gas constant, $82.06 \frac{\text{cm}^3 \text{ atm}}{\text{mol } ^\circ\text{K}}$
r	radius of cross section of body of revolution
r_0	radius of earth
T	absolute temperature, $^\circ\text{K}$
u	streamwise velocity
\bar{u}	velocity ratio, $\frac{u}{\sqrt{gr_0}}$
\bar{u}_i	entrance velocity ratio
\bar{u}_{qm}	velocity ratio at maximum heating
W	vehicle weight
X	$\frac{x}{R}$
x	distance along body surface from stagnation point
β_0	dimensionless inviscid velocity gradient at the stagnation point
Γ	nonequilibrium correlation parameter

ϵ	0 for two-dimensional body 1 for axisymmetric body
θ	nose angle, radians unless otherwise specified
μ	dynamic viscosity
ρ	density
ρ_{sl}	sea-level density
σ	Prandtl number
τ	time

Subscripts

chem	chemical
diff	diffusion
E	equilibrium
e	boundary-layer edge
f	frozen
o	stagnation point
w	wall
∞	free stream

REFERENCES

1. Chapman, Dean R.: An Analysis of the Corridor and Guidance Requirements for Supercircular Entry Into Planetary Atmospheres. NASA TR R-55, 1960.
2. Wong, Thomas J., and Slye, Robert E.: The Effect of Lift on Corridor Depth and Guidance Requirements for the Return Lunar Flight. NASA TN D-319, 1960.
3. Lees, Lester, Hartwig, Frederick W., and Cohen, Clarence B.: The Use of Aerodynamic Lift During Entry Into Earth's Atmosphere. Rep. GM-TR-0165-00519, Space Tech. Labs., Inc., 1958.
4. Slye, Robert E.: An Analytical Method for Studying the Lateral Motion of Atmosphere Entry Vehicles. NASA TN D-325, 1960.
5. Fay, J. A., and Riddell, F. R.: Theory of Stagnation Point Heat Transfer in Dissociated Air. Jour. Aero. Sci., vol. 25, no. 2, Feb. 1958, pp. 73-85, 121.
6. Lees, Lester: Convective Heat Transfer With Mass Addition and Chemical Reactions. Third AGARD Combustion and Propulsion Panel Colloquium, Palermo, Sicily, March 17-21, 1958. Pergamon Press, N. Y., pp. 451-498.
7. Lees, Lester: Laminar Heat Transfer Over Blunt-Nosed Bodies at Hypersonic Flight Speeds. Jet Propulsion, vol. 26, no. 4, Apr. 1956, pp. 259-269.
8. Kemp, Nelson H., Rose, Peter H., and Detra, Ralph W.: Laminar Heat Transfer Around Blunt Bodies in Dissociated Air. Jour. Aero/Space Sci., vol. 26, no. 7, July 1959, pp. 421-430.
9. Chung, Paul M.: Shielding Stagnation Surfaces of Finite Catalytic Activity By Air Injection in Hypersonic Flight. NASA TN D-27, 1959.
10. Chung, Paul M., and Anderson, Aemer D.: Heat Transfer Around Blunt Bodies With Nonequilibrium Boundary Layers. Proceedings of the 1960 Heat Transfer and Fluid Mechanics Institute, Stanford University 1960.
11. Demetriades, S. T., and Farlier, M.: Theoretical Study of Recombination Kinetics of Atomic Oxygen. ARS Jour., vol. 29, no. 7, July 1959, pp. 528-530.

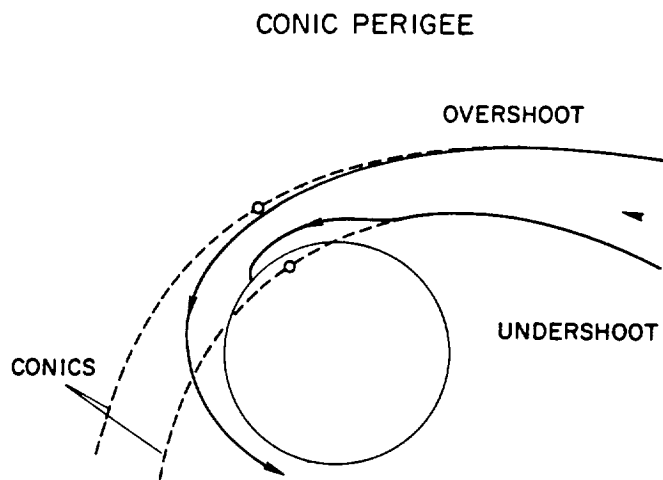


Figure 1.

CORRIDOR DEPTHS FOR LIFTING VEHICLES
 $\bar{u}_1 = \sqrt{2}$; $G_{MAX} = 10$

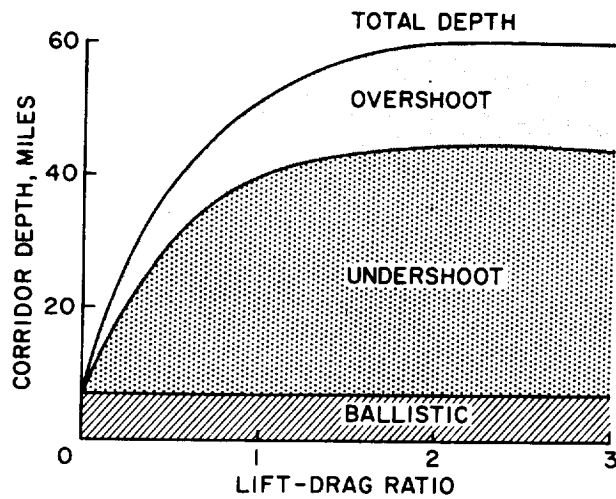


Figure 2.

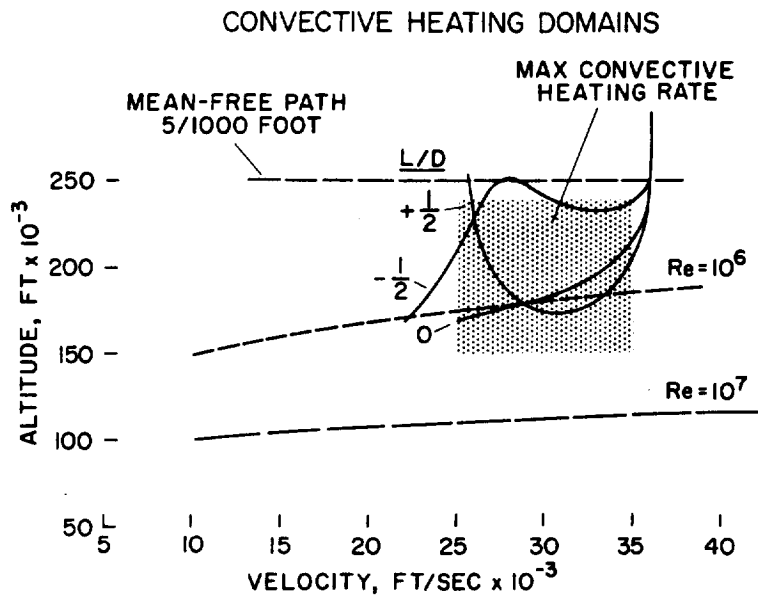


Figure 3.

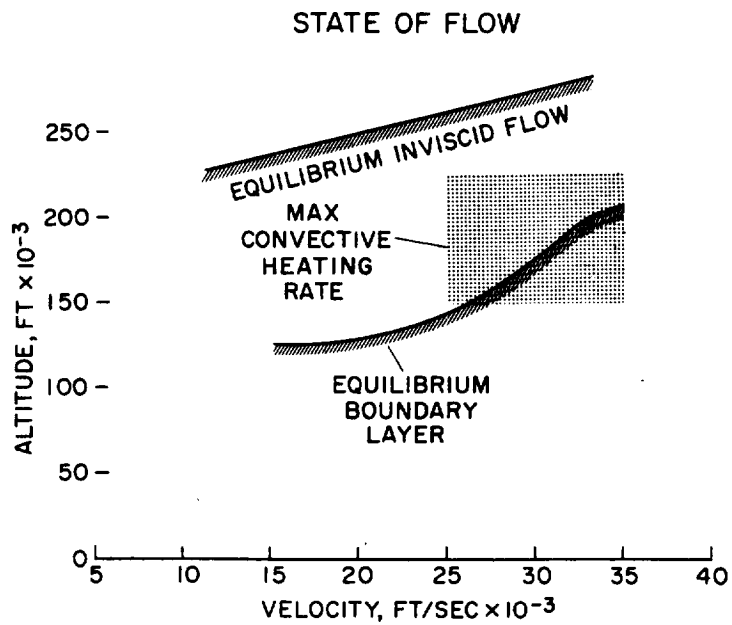


Figure 4.

HEATING HISTORIES

$$L/D = \pm \frac{1}{2}, \bar{u}_1 = \sqrt{2}, \frac{W}{C_D A R} = 56$$

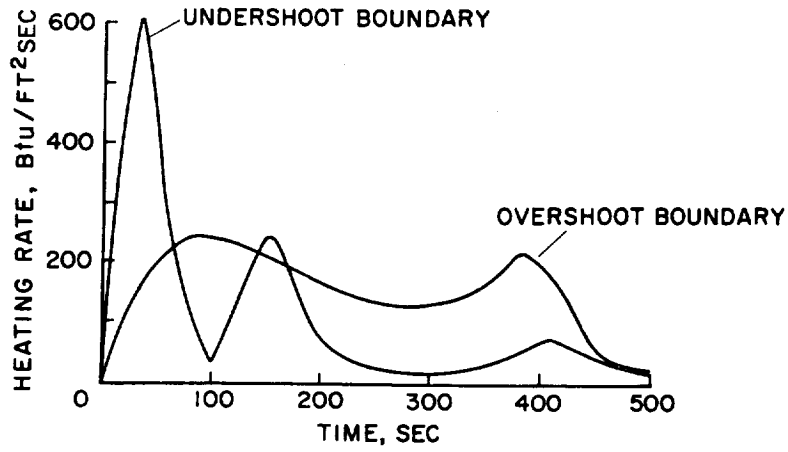


Figure 5.

HEAT-TRANSFER PARAMETER FOR FINITE RECOMBINATION RATES

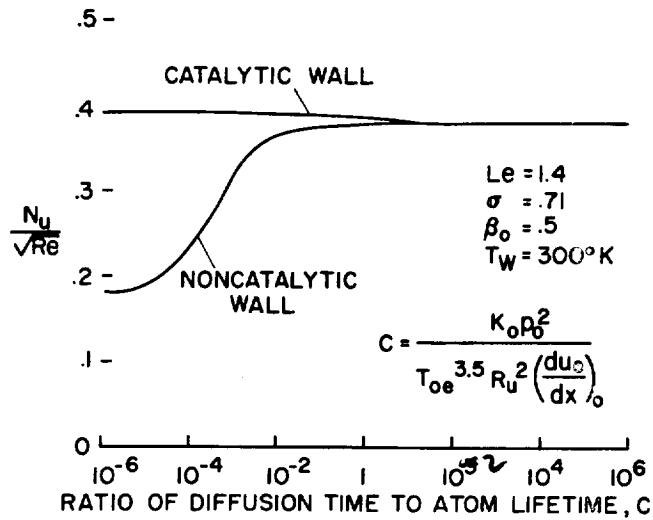


Figure 6.

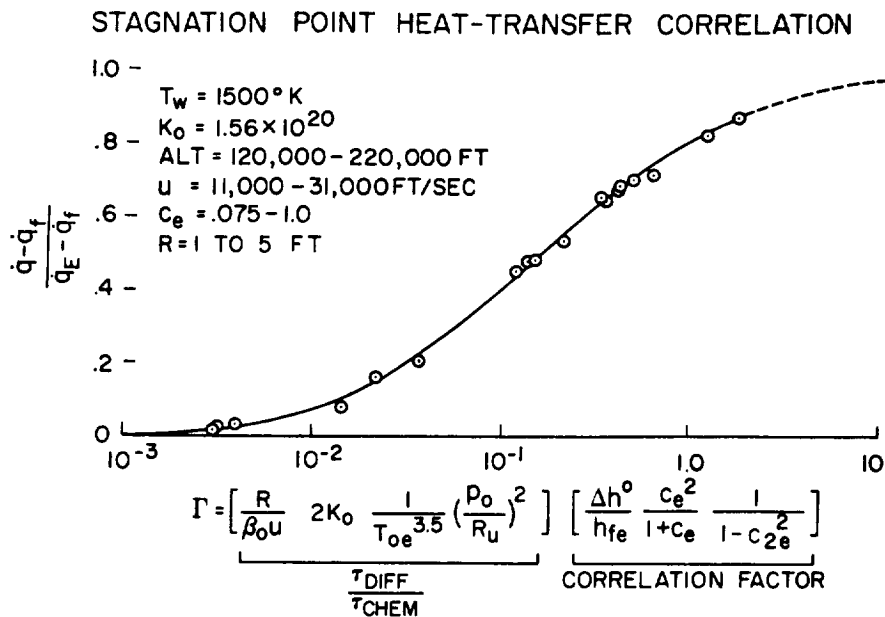


Figure 7.

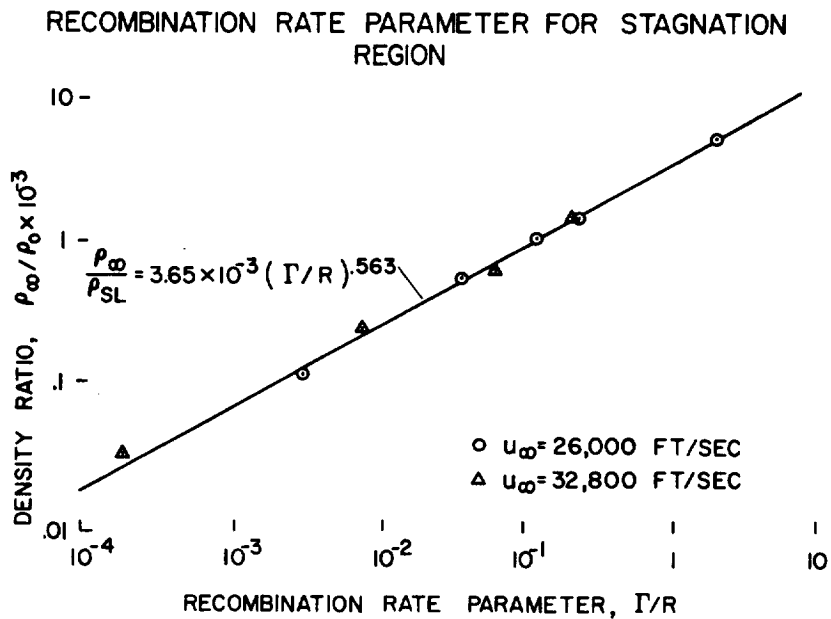


Figure 8.

EFFECT OF $\frac{W}{C_D A}$ ON STAGNATION POINT CONDITIONS

$G_{MAX}=10, L/D=0, R=5 \text{ FT}$

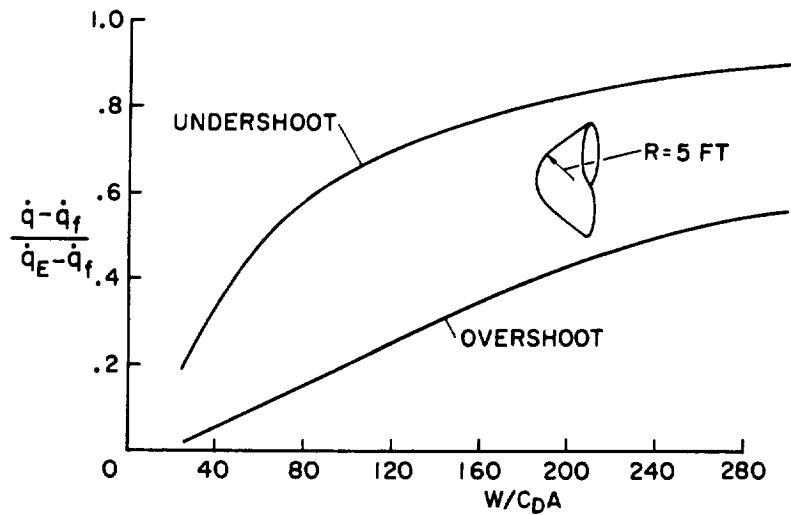


Figure 9.

EFFECT OF NOSE RADIUS ON STAGNATION POINT CONDITIONS

$\frac{W}{C_D A}=100, L/D=0, G_{MAX}=10$

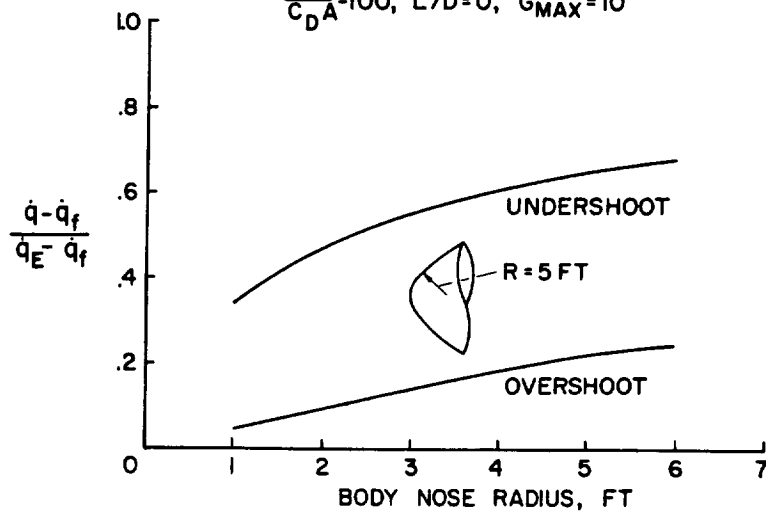


Figure 10.

EFFECT OF L/D ON STAGNATION POINT CONDITIONS

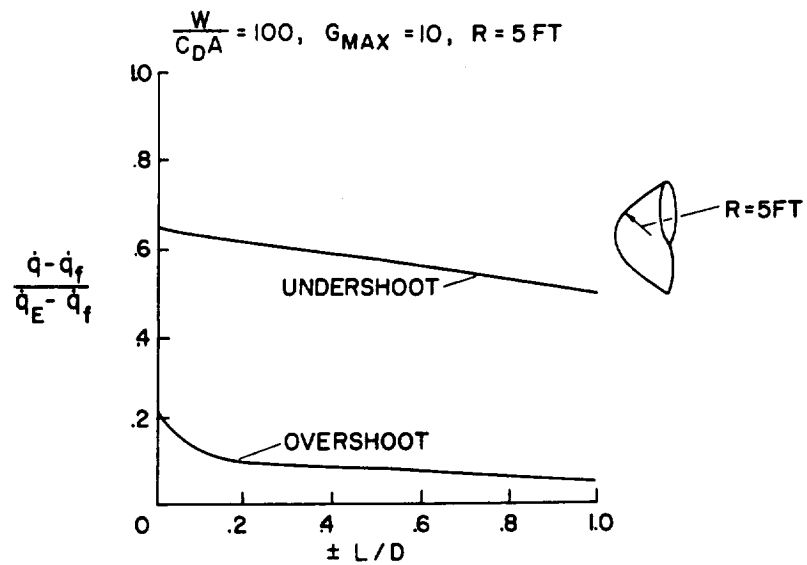


Figure 11.

HEAT-TRANSFER DISTRIBUTION

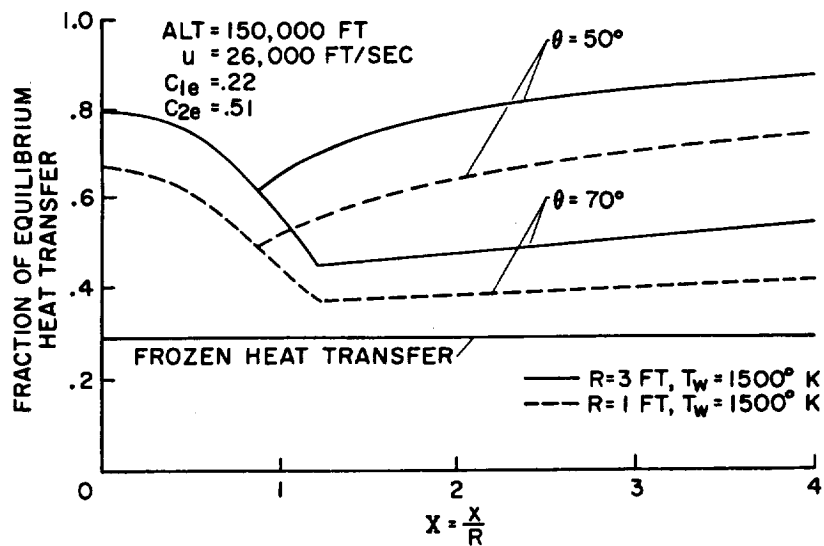


Figure 12.

CHEMICAL BEHAVIOR OF BOUNDARY LAYER AROUND THE BODY

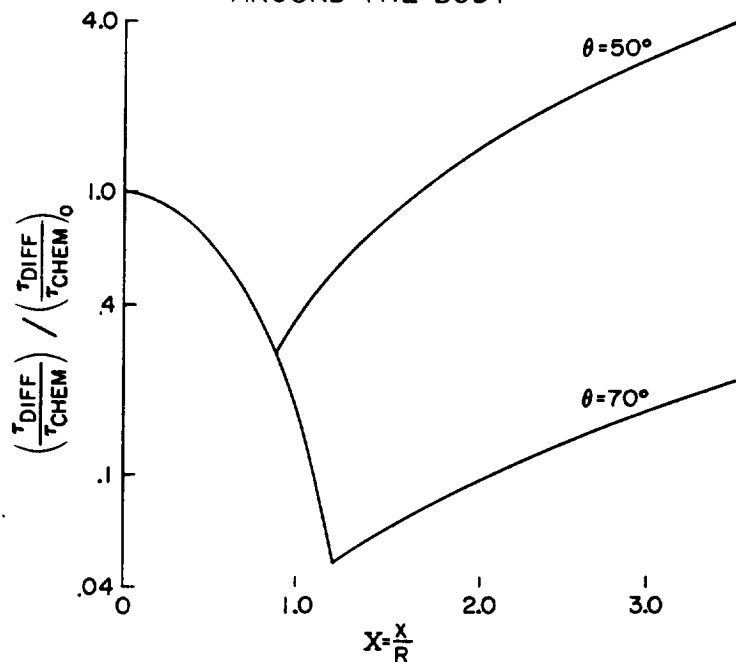


Figure 13.

SIMPLIFIED AND EXACT CALCULATIONS OF HEAT-TRANSFER DISTRIBUTION

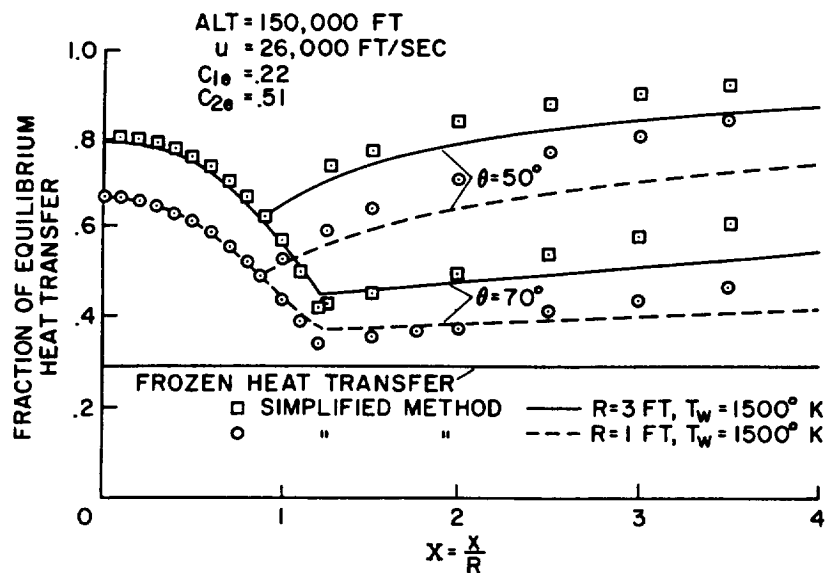


Figure 14.